

Fully Differentiable Lagrangian Convolutional Neural Network for Continuity-Consistent Physics-Informed Precipitation Nowcasting

Peter Pavlík^{1 2 3} Martin Výboh² Anna Bou Ezzeddine² Viera Rozinajová^{2 3}

Abstract

This paper presents a convolutional neural network model for precipitation nowcasting that combines data-driven learning with physics-informed domain knowledge. We propose LUPIN, a Lagrangian Double U-Net for Physics-Informed Nowcasting, that draws from existing extrapolation-based nowcasting methods and implements the Lagrangian coordinate system transformation of the data in a fully differentiable and GPU-accelerated manner to allow for real-time end-to-end training and inference. Based on our evaluation, LUPIN matches and exceeds the performance of the chosen benchmark, opening the door for other Lagrangian machine learning models.

1. Introduction

Precipitation nowcasting is the task of predicting the future intensity of precipitation (rainfall, snowfall, hail, etc.) in the near future with high local detail (WMO, 2017). The nowcasts are valuable for early warning about extreme events and can help mitigate damage and loss of lives. Accurate precipitation nowcasting can therefore increase our resilience facing the climate crisis. Radar precipitation observations from ground radar stations are good approximations of the current rainfall rate and therefore are usually used as a basis for precipitation nowcasting.

Traditionally, the nowcasting is performed using radar extrapolation methods based on the assumption that precipitation behaves and advects according to the continuity equation. A few past precipitation observations are used to estimate an advection motion field and the last observation is extrapolated forward in time according to this field. This is

the basis of many operational methods.

However, in the last few years, convolutional neural networks (CNNs) have become the de-facto state-of-the-art models for precipitation nowcasting. The first application of a CNN-based architecture in the domain was the ConvLSTM model (Shi et al., 2015). It leveraged that the problem can be posed as a spatiotemporal sequence forecasting problem similar to next-frame video prediction and therefore is a good fit for processing using CNNs.

One obvious problem with this architecture is that the convolutional recurrence structure in ConvLSTM is location-invariant, therefore not explicitly taking into consideration the advection motion of precipitation over time. This led to the development of the Trajectory GRU (TrajGRU) model (Shi et al., 2017) that can learn the location-variant structure for recurrent connections, therefore internally considering the precipitation advection. It was shown that the TrajGRU is more efficient in capturing the spatiotemporal correlations in the data.

Despite the TrajGRU model seemingly combining the best of both worlds – the physics-informed location-variant structure with data-driven CNN-based processing – location-invariant architectures continued to be developed and refined.

In (Ayzel et al., 2020), a U-Net architecture was successfully applied for precipitation nowcasting to create RainNet. Despite being a purely data-driven model without explicit inclusion of domain knowledge, it performs well and is often viewed as a simple benchmark CNN-based model.

The main challenge for all mentioned data-driven nowcasting models is the growing smoothness and fading out of the nowcasts quantities with growing time horizons. Due to the highly chaotic behavior of the precipitation in the atmosphere, there is a high degree of uncertainty in the predictions. When training with traditional gridpoint-based loss functions, we face the so-called “double penalty problem”. A forecast of a precipitation feature that is correct in terms of intensity, size, and timing, but incorrect concerning location, results in a very large error (Keil & Craig, 2009). This leads to “mathematically optimal” predictions being visibly blurry and physically inconsistent, limiting their usefulness

¹Faculty of Information Technology, Brno University of Technology, Božetěchova 1/2, Brno-Královo Pole, 612 00, Czechia
²Kempelen Institute of Intelligent Technologies, Mlynské Nivy II. 18890/5, Bratislava, 821 09, Slovakia ³Slovak Centre for Research of Artificial Intelligence - slovak.AI, Slovakia. Correspondence to: Peter Pavlík <peter.pavlik@kinit.sk>.

as nowcasts for early warning of extreme events, as those especially are smoothed out.

In an attempt to solve the blurriness challenge, some models introduced a GAN-based framework to produce realistically looking nowcasts (Tian et al., 2019; Wang et al., 2021). A notable example is the Deep Generative Model of Radar (DGMR) model (Ravuri et al., 2021) that is able to produce accurate and realistic nowcasts up to 90 minutes ahead. A visual verification by meteorologists was used, and it was selected as the best in most cases by a large margin out of all the compared nowcasting models at the time.

Recently, the GAN approach was combined with the explicit consideration of advection motion fields in NowcastNet (Zhang et al., 2023). It incorporates a differentiable evolution network that generates a motion field and performs a deterministic evolution of the precipitation according to the continuity equation before passing it to the main generative model. This helped the model outperform the DGMR by a large margin in expert evaluation at up to 3-hour ahead lead times.

Another recent model that explicitly takes into consideration the advection of the precipitation is the Lagrangian CNN (L-CNN) introduced in (Ritvanen et al., 2023). Here, the advection motion field obtained from an optical flow algorithm is used to transform the input into the Lagrangian coordinate system, where a U-Net processes the temporally differenced advection-free inputs, thus separating the learning of rainfall growth and decay from motion. The model outperformed a benchmark U-Net-based RainNet, showing that incorporating insights from rainfall physics can lead to substantial improvements in machine learning nowcasting methods. However, due to the motion field being a product of a non-differentiable optical flow method, the model can not be trained using an end-to-end approach, constraining its utility.

In this paper, we present a new model that takes inspiration from the differentiable evolution network of NowcastNet and applies it to the ingenious Lagrangian advection-free approach of LCNN to form a single end-to-end CNN-based model. We implement a differentiable semi-Lagrangian extrapolation that allows us to train the model to produce an advection motion field and dynamically map the inputs into the Lagrangian coordinates to provide a better insight for the subsequent learning of precipitation evolution by performing the Lagrangian coordinate transformation and temporal differencing during runtime. We present LUPIN: A Lagrangian Double U-Net for Physics-Informed Nowcasting.

2. The Lagrangian View

To understand the theoretical underpinnings of our approach, we first present the assumptions and methods on which the traditional nowcasting methods are based. The formalism is mostly based on the notations of (Germann & Zawadzki, 2002) and (Ritvanen et al., 2023).

2.1. Advection Equation and Lagrangian Persistence

The precipitation in the near future is highly dependent on the present weather. The basis of all traditional nowcasting methods is therefore the assumption of persistence – the precipitation in the near future will stay roughly the same as observed in the present.

In the Eulerian coordinate system, this means the simplest produced nowcast is identical to the last observation. However, the performance of this Eulerian persistence “model” falls rather quickly with increasing lead times as the current precipitation moves elsewhere.

A more realistic assumption is the Lagrangian persistence, which assumes the overall shape of the precipitation will stay the same but accounts for the displacement of the precipitation according to the advection equation. The advection equation can be expressed mathematically as follows:

$$\frac{\partial \Psi}{\partial t} + \nabla \cdot (\Psi \mathbf{u}) = 0 \quad (1)$$

where Ψ denotes the 2D radar precipitation field and \mathbf{u} the horizontal motion field. It is often assumed that the flow is incompressible, therefore the divergence of the motion field is zero (\mathbf{u} is solenoidal):

$$\nabla \cdot \mathbf{u} = 0 \quad (2)$$

Under this assumption, the advection equation (1) can be written in the form:

$$\frac{\partial \Psi}{\partial t} + \mathbf{u} \cdot \nabla \Psi = 0 \quad (3)$$

We can transform the precipitation field Ψ to a Lagrangian coordinate system precipitation field $\tilde{\Psi}$ by extrapolating it according to the motion field \mathbf{u} so that $\mathbf{u} \cdot \nabla \tilde{\Psi} = 0$ holds and the advection equation can finally be written as:

$$\frac{\partial \tilde{\Psi}}{\partial t} = 0 \quad (4)$$

The advection equation now clearly denotes the Lagrangian persistence assumption, expressing that the precipitation field in Lagrangian coordinates will not change over time.

2.2. Implementation of the Lagrangian Transformation

To transform the input 2D precipitation fields $\Psi_{1,2,\dots,n}$ to the Lagrangian coordinates $\tilde{\Psi}_{1,2,\dots,n}$, all the inputs need to be extrapolated to a single reference field. We define an extrapolation operator $\xi^t(\Psi, \mathbf{u})$ as an operation of extrapolating a precipitation field Ψ by t time steps forward in time along the motion field \mathbf{u} .

Semi-Lagrangian extrapolation (Sawyer, 1963) is commonly used as an implementation of this operator. For estimating the motion field \mathbf{u} , various optical flow methods are available, the Lucas-Kanade algorithm (Lucas & Kanade, 1981; Bouguet et al., 2001) being a popular one. Both of these are implemented in Python language in the pySTEPS nowcasting library (Pulkkinen et al., 2019).

Formally, to transform n successive input precipitation fields to Lagrangian coordinates (choosing the last one as reference), the extrapolation operator must be applied to each input image the number of times equal to the time step difference between it and the reference image:

$$\tilde{\Psi}_i = \xi^{n-i}(\Psi_i, \mathbf{u}), \quad i = 1, 2, \dots, n-1 \quad (5)$$

After this transformation, we can estimate the actual temporal difference of precipitation field from the equation (4) at a given time t as:

$$\frac{\partial \tilde{\Psi}}{\partial t} \approx \Delta \tilde{\Psi}_t = \tilde{\Psi}_t - \tilde{\Psi}_{t-1} \quad (6)$$

2.3. The Lagrangian Nowcasting

For a more realistic nowcasting of the rapidly-changing evolution of precipitation over time, we need to introduce one more term to the advection equation – a source-sink term S_Ψ which allows for the refinement of the Lagrangian persistence assumption:

$$\frac{\partial \tilde{\Psi}}{\partial t} = S_\Psi \quad (7)$$

It represents the changes in the radar precipitation field over time without considering its displacement according to the advection motion field. It can therefore be considered the the advection-free change of the field over time.

However, predicting the source-sink term S_Ψ and therefore the growth and decay of precipitation systems is very difficult. It is the biggest challenge of the nowcasting systems.

The state-of-the-art extrapolation nowcasting methods such as S-PROG (Seed, 2003), LINDA (Pulkkinen et al., 2021), STEPS (Bowler et al., 2006) and ANVIL (Pulkkinen et al., 2020) include an autoregressive model to estimate the

source-sink term S_Ψ based either on the input precipitation fields in Lagrangian coordinates $\tilde{\Psi}$ or the estimated time derivatives $\Delta \tilde{\Psi}$.

2.4. Incorporating Convolutional Neural Networks

Analogously to the autoregressive approaches, some CNN-based models have taken the Lagrangian approach to estimate source-sink term S_Ψ . In the case of TrajGRU (Shi et al., 2017), the model implicitly learns the flow field \mathbf{u} via the dynamically determined neural connections, therefore internally transforming the input fields to Lagrangian coordinates.

The L-CNN model (Ritvanen et al., 2023) takes a different approach, transforming the precipitation fields to Lagrangian coordinates before the training of the model (based on Lucas-Kanade advection motion field) and time differencing the transformed fields. Then they train a U-Net to predict the future temporal differences $\Delta \tilde{\Psi}/S_\Psi$.

Another model worth mentioning here is the Nowcast-Net (Zhang et al., 2023), specifically its Evolution Network. While it does not transform the precipitation maps to Lagrangian coordinates, it learns to separate the prediction of advection motion field from the prediction of changes in precipitation field intensity, analogous to the source-sink term S_Ψ . Also, it introduces a motion-regularization term loosely based on the continuity (advection) equation (1) to enforce a smoother motion field. In contrast to L-CNN, the differentiable evolution operator allows this model to be trainable in an end-to-end manner.

3. LUPIN – Lagrangian Double U-Net for Physics-Informed Nowcasting

This section is dedicated to introducing and describing the architecture and training process of our precipitation nowcasting model LUPIN. We compare it to previous approaches, explain the differences, and elaborate on the thought process behind them. The main point of comparison will be the Lagrangian CNN (L-CNN) model from (Ritvanen et al., 2023), as it served as the main inspiration for our approach, whose shortcomings we aim to address.

3.1. LUPIN Architecture

The overall architecture of the LUPIN model is based on the architecture of the LCNN model (Ritvanen et al., 2023). We took the key idea of the L-CNN – to transform the input data to Lagrangian coordinates and use a CNN to model the time derivatives of rainfall fields (the source-sink term $S_\Psi = \Delta \tilde{\Psi}_{t+1}$) – and decided to explore implementing this approach as a fully data-driven model.

The inclusion of the optical flow algorithm in the L-CNN

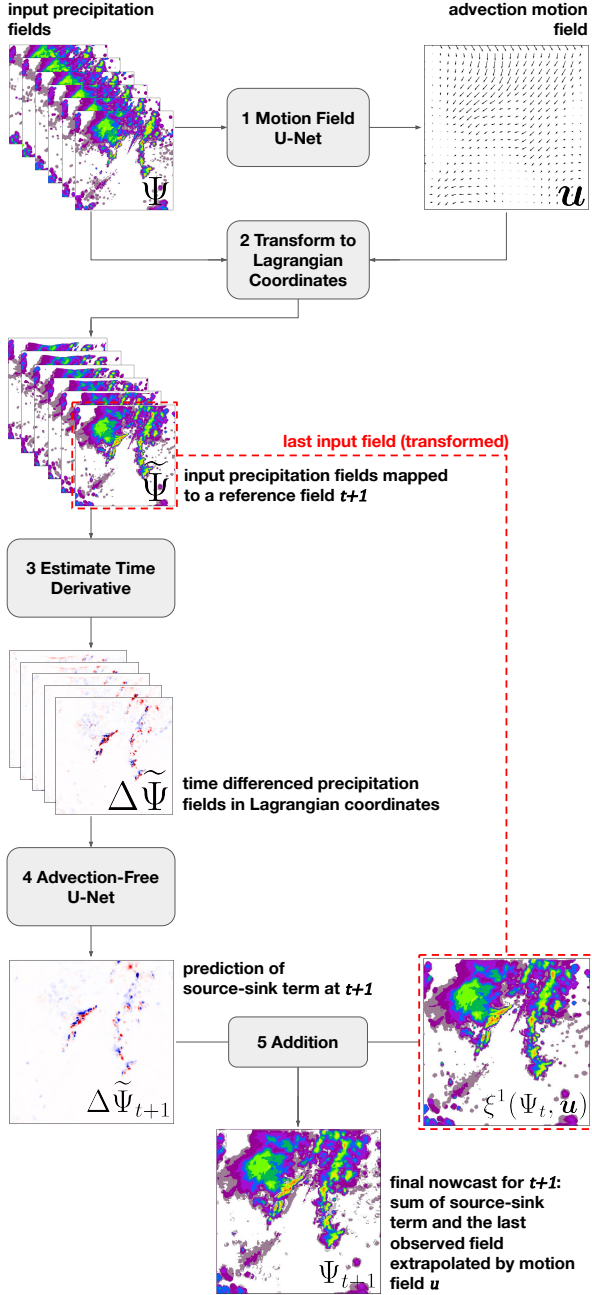


Figure 1. Architecture of the LUPIN model and the inference process of a nowcast one time step ahead. The gray processing blocks are marked 1 to 5 in the order they are called during inference. **1** The first step is the calculation of the advection motion field u . **2** Then, the input fields Ψ can be transformed into Lagrangian coordinates as described in Equation 5. **3** The precipitation maps in Lagrangian coordinates are differenced over time to obtain $n-1$ time differenced fields $\Delta \tilde{\Psi}$. **4** The differenced fields are used as an input to the Advection-Free U-Net that predicts the next differenced field $\Delta \tilde{\Psi}_{t+1}$ (representing the source-sink term S_Ψ at time $t+1$). **5** The predicted source-sink term is added to the last input field (already transformed in step 2 to reference field $t+1$), the product being the final nowcast for the next time step.

model makes the training process cumbersome. The algorithm is orders of magnitude slower compared to the time needed for GPU-accelerated inference and backpropagation in a CNN. This makes the training feasible only with inputs and outputs transformed to Lagrangian coordinates beforehand. At the same time, the longer inference limits the application of the model for ensemble nowcasting.

Our solution was to implement a differentiable semi-Lagrangian-like extrapolation operation in the PyTorch machine learning framework (Paszke et al., 2019). This allowed us to create a model that learns to produce the motion field in a data-driven manner and then performs the transformation to Lagrangian coordinates dynamically during runtime in a fraction of the time.

The overall LUPIN architecture is in the form of a double U-Net, see Figure 1. The first U-Net (Motion Field U-Net) produces the motion fields and functionally replaces the Lukas-Kanade optical flow algorithm in the L-CNN. The second one (Advection-free U-Net) works with the Lagrangian-transformed and time differenced inputs analogous to the L-CNN specification.

The model is to be applied iteratively in a rolling window manner. Each inference produces a new motion field and the corresponding nowcast for the next time step. The nowcast then subsequently serves as the last input observation for the next iteration. By choosing the reference time for the Lagrangian mapping to match the one-step ahead nowcast window $t+1$, we have eliminated the need to perform the transformation back to Eulerian coordinates as the final prediction step, simplifying the inference process in comparison to the L-CNN.

3.2. Training Process

Training the LUPIN is a three-stage process. While it is feasible to train the whole model at once, preliminary experiments have shown this to be unstable. We therefore used the following process:

1. Train the Motion Field U-Net (MF-U-Net) to produce satisfactory motion fields by itself.
2. Train the Advection-Free U-Net (AF-U-Net) with the MF-U-Net’s weights frozen.
3. Train both U-Nets together to act jointly as a single model.

3.2.1. TRAINING MF-U-NET

Training the MF-U-Net to produce physically consistent advection motion fields u is not trivial. To be usable in the Lagrangian framework, the motion fields should be stable over time when produced iteratively and smooth so as to

not interfere in the subsequent estimation of temporal differences in Lagrangian coordinates. We want to emulate a simple Lagrangian persistence model in a data-driven way.

The first intuitive approach was to just minimize the error between the last input observation extrapolated by one time step and the ground truth. We denote the error criterion \mathcal{C} and the target precipitation field $\hat{\Psi}$.

$$\mathcal{L}_{naive} = \mathcal{C}(\xi^1(\Psi_t, \mathbf{u}), \hat{\Psi}_{t+1}) \quad (8)$$

However, regardless of the criterion \mathcal{C} , this loss function produces highly unrealistic motion fields full of sinks and sources, functionally interfering with the future task of the AF-U-Net. It goes against the assumption described by Equation 2 of the divergence-free motion field for the Lagrangian persistence.

To mitigate this, we produce a pooled optimal motion field by minimizing the error of extrapolating the precipitation fields by one-time step over the whole input sequence.

$$\mathcal{L}_{MF} = \sum_{t=1}^n \mathcal{C}(\xi^1(\Psi_t, \mathbf{u}), \hat{\Psi}_{t+1}), \quad n = ||\Psi|| \quad (9)$$

This loss function iterates over all n input observations and sums the error of extrapolating them one step forward in time. This pushes the model to produce more stable motion fields better fit for transforming the inputs into the Lagrangian coordinate system.

In addition, we introduce a physics-informed regularization loss to directly penalize breaking the Equation 2. By enforcing it, we can push the model towards creating solutions consistent with the continuity equation derived from conservation laws. The assumption is also one of the Navier-Stokes partial differential equations that govern fluid dynamics (Batchelor, 1967). Since our data captures the movement of air in the atmosphere, it should behave according to these equations. The regularization will therefore make the motion fields more physically consistent.

The divergence $\nabla \mathbf{u}$ is calculated using partial derivatives of the motion field:

$$\nabla \mathbf{u} = \frac{\partial u_x}{\partial x} + \frac{\partial u_y}{\partial y} \quad (10)$$

We can compute discrete approximations of motion field partial derivatives using 2D convolutions with a 3×3 Sobel filter.

a)	$\begin{bmatrix} -1 & 0 & 1 \\ -2 & 0 & 2 \\ -1 & 0 & 1 \end{bmatrix}$	b)	$\begin{bmatrix} -1 & 2 & -1 \\ 0 & 0 & 0 \\ 1 & 2 & 1 \end{bmatrix}$
----	--	----	---

The filter a) is used to estimate $\frac{\partial u_x}{\partial x}$ and the filter b) estimates $\frac{\partial u_y}{\partial y}$. Using these values, we define the physics-informed continuity-consistency loss function at every point of the motion field as:

$$\mathcal{L}_{PI} = |\nabla \mathbf{u}| \quad (11)$$

In the vocabulary of physics-informed machine learning, this is a soft constraint or learning bias, meaning we allow the network to break the constraint, but penalize it as it diverges.

The final loss function that is minimized is simply the weighted sum of the data-driven and physics-informed losses:

$$\mathcal{L} = (1 - \beta)\mathcal{L}_{MF} + \beta\mathcal{L}_{PI} \quad \beta \in (0, 1) \quad (12)$$

3.2.2. TRAINING AF-U-NET

The second training stage starts with taking the pre-trained MF-U-Net and freezing the weights, so as not to unlearn the motion field generation from unstable gradients being backpropagated from the downstream AF-U-Net. Because the MF-U-Net has been trained to effectively perform the Lagrangian persistence nowcasting, we can train the AF-U-Net to post-process its predictions by learning to produce a source-sink term S_Ψ capturing the growth and decay of precipitation fields over time.

As shown in the L-CNN paper, the Lagrangian-transformed and time-differenced fields can allow the Advection-Free U-Net to better grasp the precipitation growth and decay in the data, resulting in more accurate predictions with less blurring as lead time increases. Therefore, the input fields to our Advection-Free U-Net are also being transformed and time-differenced. The Lagrangian transformation is performed dynamically during training using our implementation of the semi-Lagrangian extrapolation.

The prediction task the Advection-Free U-Net performs is in essence auto-regressive, as the target output (source-sink term $S_{\Psi_{t+1}} = \Delta \Psi_{t+1}$) is the expected difference of the last input extrapolated by one time step ($\xi^1(\Psi_t, \mathbf{u})$) from the ground truth observation ($\hat{\Psi}_{t+1}$). To obtain the nowcast for the next time step, a simple addition of these fields is performed:

$$\Psi_{t+1} = S_{\Psi_{t+1}} + \xi^1(\Psi_t, \mathbf{u}) \quad (13)$$

The error of this nowcast in relation to the observed precipitation field target forms the loss function during this training stage:

$$\mathcal{L}_{AF} = \mathcal{C}(\Psi_{t+1}, \hat{\Psi}_{t+1}) \quad (14)$$

In a way, this can be viewed as a form of residual learning, with the output of the AF-U-Net serving as a residual being added to a single skip-connected input channel.

3.2.3. TRAINING LUPIN

By training the models only separately, an issue of out-of-distribution samples arises. The AF-U-Net produces nowcasts that get blurrier as lead time increases due to uncertainty. This means that, eventually, the outputs do not look like the input images the model was trained on. This poses a problem for the MF-U-Net which is given input data that does not look like the data it was trained on, resulting in unstable advection motion fields.

Therefore, for these models to cooperate together, a final stage of training is needed. This fine-tuning stage is mostly similar to the previous one. The only change is that we unfreeze the weights of the MF-U-Net and add its loss functions to the total loss function being minimized.

In this training stage, the MF-U-Net parameters are updated not only by the gradients backpropagated from the loss function described in Equation 12, but also the gradients from the AF-U-Net due to the differentiable implementation of the whole LUPIN model. We hypothesize that this might allow the model to produce more useful advection motion fields than the general optical flow algorithms, as the model is trained specifically to produce motion fields for the optimal Lagrangian coordinate transformation of the precipitation fields.

The total weighted loss optimized in this stage, consisting of the three separate weighted loss terms, is specified as:

$$\mathcal{L} = (1 - \beta)((1 - \gamma)\mathcal{L}_{AF} + \gamma\mathcal{L}_{MF}) + \beta\mathcal{L}_{PI} \quad \beta, \gamma \in (0, 1)$$

4. The Precipitation Dataset

For training the LUPIN model, we use a dataset provided by the Slovak Hydrometeorological Institute (SHMU). The dataset consists of radar reflectivity observations from the 1st of January 2016 until the 30th of June 2019, collected periodically in 5-minute intervals. Data originates from Malý Javorník weather radar station, located in the Carpathian Mountains in Western Slovakia. The dataset contains 355761 unique observations in ODIM HDF5 format.

The data is processed from raw radar reflectivity observations to Cartesian coordinates using the Py-ART Python library (Helmus & Collis, 2016). We aggregate the 3-dimensional precipitation observations into a single two-dimensional reflectivity map by a method called CMAX.

It groups data by returning the maximum value of reflectivity in the vertical column. Resulting reflectivity map is a 340km \times 340km sized center slice with 1km \times 1km resolution. The reflectivity is converted to rainfall rate, measured in mm/h, using Marshall-Palmer formula (Marshall & Palmer, 1948):

Theorem 4.1. *For the reflectivity factor Z and rainfall rate R in mm h⁻¹ holds the equation $Z = 200R^{1.6}$, where 200 and 1.6 are empirically derived constants.*

4.1. Dataset filtering

To prevent training the neural network on a biased dataset that contains mostly observations with no precipitation, subsetting the full dataset is necessary. Keeping observations of clear skies in the dataset might negatively affect resulting nowcasts, causing overfitting to observations containing no precipitation activity.

To filter the images, we convert CMAX reflectivity maps to rainfall rate, using the Marshall-Palmer formula from Theorem 4.1. Then, we compute the ratio of rainy to clear pixels in the map with the threshold of 0.05mm/5min or 0.6mm h⁻¹. Finally, if the rainfall rate map contains at least 5% of rainy pixels and 11 previous observations are available (last hour), it is added to the target observations set.

For training LUPIN, we decided to use 6 input observations and 6 output observations, therefore, for predicting the target observation, 11 lead observations are needed to be kept in the dataset.

The dataset is split into train, test, and validation subsets. The last 20% of target observations are selected for the test set. This set contains rainfall maps from the 2nd of September 2018 until the 30th June of 2019. The first 80% of the data is chosen for training, out of which 15% is split further into a validation set.

The training set is split randomly into training and validation subsets, ensuring that there are no overlapping observations in these sets (e.g. there are no target observations in the training set that are lead observations for the validation set and vice versa). The exact observation counts can be observed in Table 1.

5. Evaluation

This section presents qualitative and quantitative results of the LUPIN training in comparison to selected reference models. As mentioned in Section 1, a visual qualitative comparison of produced nowcasts in an expert study is often more valuable than comprehensive quantitative evaluation, as there is no clear numerical metric that measures the fitness of nowcasts.

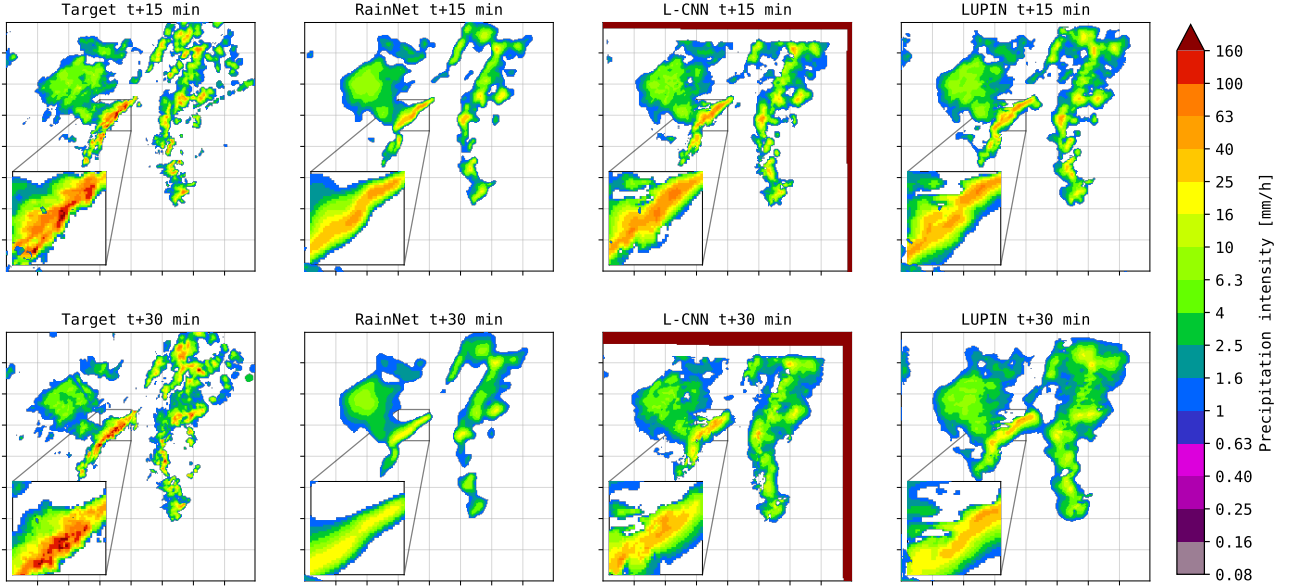


Figure 2. Extreme event example from the evening of September 2nd, 2018. The leftmost column shows radar rainfall fields of a growing convective rain cell, with the maximum rain rate region zoomed in. Precipitation below 1 mm/h was filtered out. The other columns show nowcasts of the respective target fields at two lead times: $t + 15$ and $t + 30$ minutes. All the models are able to capture the general southwestern movement of the precipitation field. However, the models show blurring of the output over time due to uncertainty.

Table 1. The observation counts of the full dataset, the subset selected for training according to the dataset filtering described in Section 4.1, and the sizes of train, test, and validation splits.

SET	N° OBS.	FULL %	TARGET %
FULL DATASET	355761	100.00	-
TARGET & LEAD OBS.	63007	17.71	-
TARGET OBS.	54721	15.38	100.00
TARGET OBS. TRAIN.	35767	10.05	65.37
TARGET OBS. VALID.	7998	2.25	14.61
TEST TARGET OBS.	10956	3.08	20.02

5.1. Reference Models

The main model to compare against is naturally L-CNN, the model LUPIN was based on. The performance of LUPIN needs to at least match the performance of the L-CNN, or, if our data-driven Lagrangian coordinate transformation is better, exceed it.

The second reference model chosen is RainNet, a U-Net-based nowcasting model. The architecture matches the AF-U-Net in LUPIN but is a pure machine learning model with no Lagrangian assumptions. It is therefore a good benchmark, as its performance will show us the benefits gained from the Lagrangian approach.

The task of all three models is to take 6 successive precip-

itation fields and iteratively predict the next 6 fields. All the compared models have the same back-end structure – an identical U-Net. Any differences observed are therefore the consequence of the different training regimes and data transformations.

5.2. Extreme event case study

On September 2nd, 2018, southwest Slovakia was hit by a severe convective storm. It flooded underpasses, streets, and basements of buildings and caused public transport collapse in the capital of Slovakia (ESSL, 2023). The convective storms are complex and hard to predict. They are the most relevant cause of systematic errors in weather and climate models (Reynolds et al., 2020). This rainfall event from the test set was chosen to compare the performance of selected nowcasting models. See Figure 2 for the nowcasts produced by the models.

The RainNet model exhibits very strong blurring of the output with growing lead time. In comparison, both the L-CNN and LUPIN produce less blurry outputs of similar local detail that better preserve the expected high precipitation intensity, more closely resembling the target precipitation field. The benefits of the Lagrangian approach are clearly visible.

5.3. Quantitative Comparison

To compare the models quantitatively, their performance is evaluated using multiple different metrics over the whole test set. The quantitative results are presented grouped by lead time to get a better idea about the models' behavior with increasing lead times. First, for the computed mean square error (MSE) and mean bias error (ME), see Figure 3.

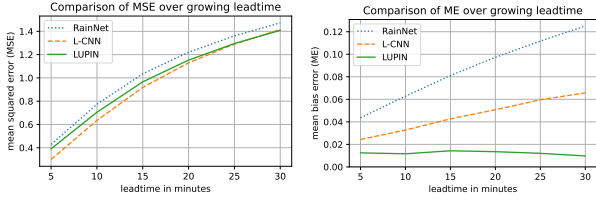


Figure 3. Plots show the test set MSE (left) and ME (right) of the compared models in relation to nowcast lead time.

The L-CNN performs the best in terms of MSE, though with growing lead times LUPIN catches up. LUPIN also shows the least model bias (ME), constantly being close to zero even with growing lead time.

To better evaluate the performance of the models at predicting high precipitation events, we also calculate three binary classification metrics over binary rainfall fields with a threshold of 10 mm/h. We calculate precision and recall of the models along with equitable threat score, a common indicator of warning skill in weather forecasting (Schaefer, 1990). See Figure 4 for comparison.

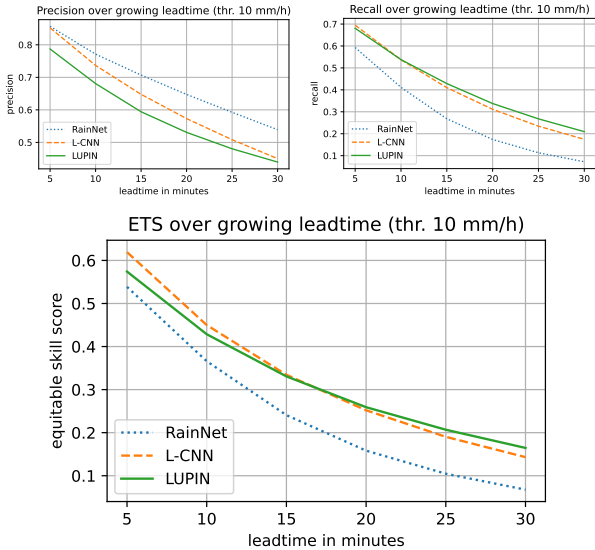


Figure 4. Plots show test set precision (top left), recall (top right), and equitable threat score (bottom) of the compared models in relation to nowcast lead time.

Precision – a complement of false alarm ratio (FAR) – marks

the probability that a positive prediction (an alarm) is really a positive. In this metric, the RainNet naturally leads due to its blurring. When it produces an alarm, there is a high chance of it being true. This shows that precision is not really a high priority as a metric for a warning system.

On the other hand, recall – also called the probability of detection (POD) – signifies the probability that a true positive (an extreme event) will, in fact, trigger a positive prediction (an alarm). In the context of a warning system, this metric is of high priority to minimize the amount of missed events. Here, L-CNN and LUPIN both perform much better than RainNet. With increasing lead time, LUPIN achieves better recall compared to L-CNN, with more than 20 % better recall at the $t + 30$ minutes lead time.

Finally, the equitable threat score (ETS) – based on the frequently used critical success index (CSI) – considers both the false alarms and the missed events, while also taking into account hits expected by chance. Here, the RainNet also falls far behind the Lagrangian models. According to this metric, the L-CNN performs better at the start, but LUPIN again outperforms it with increasing lead times, still ending up with almost 15 % better performance at the final lead time.

6. Conclusion

By implementing the temporal differencing applied to rainfall fields in Lagrangian coordinates introduced by the L-CNN in a fully differentiable manner, we have eliminated most of the drawbacks of the original model, while matching or even slightly exceeding its performance in our evaluation.

Thanks to our implementation of the semi-Lagrangian extrapolation and training the data-driven MF-U-Net to produce physically consistent advection motion fields dynamically during runtime, we mitigate the higher computational cost at the inference of the L-CNN model. The MF-U-Net also mitigates the dependence on the quality of the motion field generated by optical flow methods that can be impacted by edge effects or gaps in radar coverage in the precipitation fields.

The quality of LUPIN's transformation to Lagrangian coordinates in comparison to L-CNN is hard to quantify, however, it is possibly better due to the temporally varying motion field at each iteration as opposed to L-CNN's static one. This might be the cause of better performance with increasing lead time observed in MSE, recall, and ETS metrics compared to the L-CNN.

The LUPIN framework, as defined in this paper, is flexible and not tied to any specific neural network architecture. With the generative models achieving great results in the precipitation nowcasting domain in recent years, our work

opens the possibility of them leveraging the Lagrangian approach efficiently. We believe that including domain knowledge and physical laws in the machine learning models is necessary to build more trustworthy and reliable models for the future.

Ethical Impacts and Expected Societal Implications

This paper presents work whose goal is to advance the field of machine learning. There are many potential societal consequences of our work, none of which we feel must be specifically highlighted here.

Acknowledgments

This research was partially supported by TAILOR, a project funded by EU Horizon 2020 research and innovation programme under GA No 952215.

References

- Ayzel, G., Scheffer, T., and Heistermann, M. Rainnet v1. 0: a convolutional neural network for radar-based precipitation nowcasting. *Geoscientific Model Development*, 13(6):2631–2644, 2020.
- Batchelor, G. K. *An introduction to fluid dynamics*. Cambridge university press, 1967.
- Bouquet, J.-Y. et al. Pyramidal implementation of the affine lucas kanade feature tracker description of the algorithm. *Intel corporation*, 5(1-10):4, 2001.
- Bowler, N. E., Pierce, C. E., and Seed, A. W. Steps: A probabilistic precipitation forecasting scheme which merges an extrapolation nowcast with downscaled nwp. *Quarterly Journal of the Royal Meteorological Society: A journal of the atmospheric sciences, applied meteorology and physical oceanography*, 132(620):2127–2155, 2006.
- ESSL. European severe weather database, 2023. URL <https://eswd.eu/queries/21365.html>.
- Germann, U. and Zawadzki, I. Scale-dependence of the predictability of precipitation from continental radar images. part i: Description of the methodology. *Monthly Weather Review*, 130(12):2859–2873, 2002.
- Helmus, J. J. and Collis, S. M. The python arm radar toolkit (py-art), a library for working with weather radar data in the python programming language. *Journal of Open Research Software*, 4(1):e25, 2016. URL <http://doi.org/10.5334/jors.119>.
- Keil, C. and Craig, G. C. A displacement and amplitude score employing an optical flow technique. *Weather and Forecasting*, 24(5):1297 – 1308, 2009. doi: 10.1175/2009WAF2222247.1. URL https://journals.ametsoc.org/view/journals/wefo/24/5/2009waf2222247_1.xml.
- Lucas, B. D. and Kanade, T. An iterative image registration technique with an application to stereo vision. In *IJCAI’81: 7th international joint conference on Artificial intelligence*, volume 2, pp. 674–679, 1981.
- Marshall, J. S. and Palmer, W. M. K. The distribution of raindrops with size. *Journal of the Atmospheric Sciences*, 5(4):165–166, 1948. URL [https://doi.org/10.1175/1520-0469\(1948\)005<0165:TDORWS>2.0.CO;2](https://doi.org/10.1175/1520-0469(1948)005<0165:TDORWS>2.0.CO;2).
- Paszke, A., Gross, S., Massa, F., Lerer, A., Bradbury, J., Chanan, G., Killeen, T., Lin, Z., Gimelshein, N., Antiga, L., et al. Pytorch: An imperative style, high-performance deep learning library. *Advances in neural information processing systems*, 32, 2019.
- Pulkkinen, S., Nerini, D., Pérez Hortal, A. A., Velasco-Forero, C., Seed, A., Germann, U., and Foresti, L. Pysteps: an open-source python library for probabilistic precipitation nowcasting (v1.0). *Geoscientific Model Development*, 12(10):4185–4219, 2019. doi: 10.5194/gmd-12-4185-2019. URL <https://gmd.copernicus.org/articles/12/4185/2019/>.
- Pulkkinen, S., Chandrasekar, V., von Lerber, A., and Harri, A.-M. Nowcasting of convective rainfall using volumetric radar observations. *IEEE Transactions on Geoscience and Remote Sensing*, 58(11):7845–7859, 2020.
- Pulkkinen, S., Chandrasekar, V., and Niemi, T. Lagrangian integro-difference equation model for precipitation nowcasting. *Journal of Atmospheric and Oceanic Technology*, 38(12):2125–2145, 2021.
- Ravuri, S., Lenc, K., Willson, M., Kangin, D., Lam, R., Mirowski, P., Fitzsimons, M., Athanassiadou, M., Kashem, S., Madge, S., et al. Skilful precipitation nowcasting using deep generative models of radar. *Nature*, 597(7878):672–677, 2021.
- Reynolds, C., Williams, K. D., and Zadra, A. Wgne systematic error survey results summary. In *100th American Meteorological Society Annual Meeting*. AMS, 2020.
- Ritvanen, J., Harnist, B., Aldana, M., Mäkinen, T., and Pulkkinen, S. Advection-free convolutional neural network for convective rainfall nowcasting. *IEEE Journal of Selected Topics in Applied Earth Observations and Remote Sensing*, 16:1654–1667, 2023. doi: 10.1109/JSTARS.2023.3238016.

- Sawyer, J. S. A semi-lagrangian method of solving the vorticity advection equation. *Tellus*, 15(4):336–342, 1963.
- Schaefer, J. T. The critical success index as an indicator of warning skill. *Weather and forecasting*, 5(4):570–575, 1990.
- Seed, A. A dynamic and spatial scaling approach to advection forecasting. *Journal of Applied Meteorology and Climatology*, 42(3):381–388, 2003.
- Shi, X., Chen, Z., Wang, H., Yeung, D.-Y., Wong, W.-K., and Woo, W.-c. Convolutional lstm network: A machine learning approach for precipitation nowcasting. *Advances in neural information processing systems*, 28, 2015.
- Shi, X., Gao, Z., Lausen, L., Wang, H., Yeung, D.-Y., Wong, W.-k., and Woo, W.-c. Deep learning for precipitation nowcasting: A benchmark and a new model. *Advances in neural information processing systems*, 30, 2017.
- Tian, L., Li, X., Ye, Y., Xie, P., and Li, Y. A generative adversarial gated recurrent unit model for precipitation nowcasting. *IEEE Geoscience and Remote Sensing Letters*, 17(4):601–605, 2019.
- Wang, C., Wang, P., Wang, P., Xue, B., and Wang, D. Using conditional generative adversarial 3-d convolutional neural network for precise radar extrapolation. *IEEE Journal of Selected Topics in Applied Earth Observations and Remote Sensing*, 14:5735–5749, 2021.
- WMO. *Guidelines for Nowcasting Techniques*. Number 978-92-63-11198-2. World Meteorological Organization, 7 bis, avenue de la Paix, P.O. Box 2300, CH-1211 Geneva 2, Switzerland, 2017.
- Zhang, Y., Long, M., Chen, K., Xing, L., Jin, R., Jordan, M. I., and Wang, J. Skilful nowcasting of extreme precipitation with nowcastnet. *Nature*, 619(7970):526–532, 2023.